JJEES

JJEES (2024) 15 (1): 20-27
ISSN 1995-6681

Jordan Journal of Earth and Environmental Sciences

Geochemical Characteristics of Rare Earth Elements in Argillic Alteration Zone: An Example from the Kharvana area, NW Iran

Ali Abedini[1*] and Maryam Khosravi[2]

[1] Urmia University, Geology Department, Faculty of Sciences, Urmia, Iran
[2] Isfahan University of Technology, Department of Mining Engineering, Isfahan, Iran

Received April 17, 2023; Accepted September 12, 2023

Abstract

The emplacement of Oligocene tonalitic, granodiorite, and quartz diorite suites into Cretaceous andesitic rocks causes the generation of an argillic alteration zone in the northeast of the Kharvana area. No detailed geochemical consideration of the argillic alteration zone has been carried out. In this research, factors controlling the mobility and concentration of rare earth elements (REE) in this alteration zone are determined by different geochemical techniques. The mineralogical and geochemical characteristics of the argillic alteration zone were examined by X-ray diffractometer and Inductively Coupled Plasma-Atomic Emission Spectrometry (ICP–AES) and Inductively Coupled Plasma-Mass Spectrometry (ICP–MS), respectively. Based on mineralogical analyses, quartz, kaolinite, alunite, pyrophyllite, muscovite–illite, rutile, chlorite, jarosite, hematite, goethite, and pyrite are the dominant mineral phases in the Kharvan argillic alteration zone. Chondrite-normalized REE spider diagrams indicate fractionation and enrichment of LREE from HREE, along with Eu and Ce negative anomalies during the development of the argillic alteration zone. Taking into account Al as an immobile monitor element, argillization of andesite rocks was accompanied by leaching and fixation of REE. Whereas, among the lanthanides, Ce displays a decrease in the content of all the argillic samples. Combining the results obtained from mass change calculations and geochemical parameters, such as $(\Sigma LREE/\Sigma HREE)_N$ and $(La/Yb)_N$ ratios, shows that the distribution of lanthanides during the development of the argillic alteration zone is controlled by a number of factors, including changes in pH and redox potential of environment, the difference in the degree of destabilization of lanthanide complexes, adsorption, scavenging by metallic oxides and hydroxides, and isomorphic substitution.

Keywords: *Argillic alteration; Mobility; Rare earth elements; Kharvana; Northwestern Iran.*

1. Introduction

The mobility, distribution, and fractionation of rare earth elements (REE) during alteration processes in different environments have been documented by several researchers and have been used to determine the chemistry of solutions responsible for alteration and mineralization (Dill et al., 1997; Galan et al., 1998; El-Hasan et al., 2008; El-Hasan and Al-Malabeh, 2008; Parsapoor et al., 2009; Karakaya, 2009; Cravero et al., 2010; Karakaya et al., 2012; Grecco et al., 2012; Siahcheshm et al., 2014; Ercan et al., 2016; Al Smadi et al., 2018; Abedini et al., 2020; Kadir et al., 2022; Abd El-Moghny et al., 2022; Garofalo et al., 2023). The REE mobility is significantly controlled by the availability of complexing ions, such as F^-, Cl^-, CO_3^{-2}, PO_4^{3-}, and SO_4^{2-}, low pH, and high rock/fluid ratios as well (Wood, 1990; Haas et al., 1995; Fulignati et al., 1999; Seewald et al., 2019). In addition, many studies that focused on pertaining the significance of REE for exploration have been used (Qi-Cong and Cong-Qiang, 2002; Weimin et al., 2003; Abedini and Calagari, 2012; Tassongwa et al., 2017; Apollaro et al., 2023). Based on these researches, the ore bodies prospective for metal mineralization might have a distinctive REE signature and, therefore, they may have some applications for exploration (Dill et al., 2015). It suggests that REE behavior in a hydrothermal environment is complex and no simple rules can address the mobility and fractionation of REE during hydrothermal processes (Parsapoor et al., 2009; Rezaei Azizi et al., 2018a, b).

It is believed that the Alborz–Azarbaidjan Mountains and magmatic events in the northwestern part of Iran are a result of the collision of the Gondwana and Arabian Plate with the Eurasian Plate during the late Cretaceous–early Paleogene. This phenomenon causes the development of an extensional basin in the northwestern part of Iran (Mollai et al., 2014; Simmonds et al., 2015; Abedini et al., 2018; Ghasemi Siani and Lentz, 2022). The Cenozoic Ahar–Arasbaran volcanic belt (hereafter AHAVB) in northwestern Iran includes numerous ore deposits and different mineralization types, such as porphyry, Cu–Fe skarn, and epithermal deposits (e.g. Mollai et al., 2014; Jamali and Mehrabi, 2015). The AHAVB, about 100 km wide, extends from NW Iran to Armenia and the eastern Pontide arc in NE Turkey (Jamali et al., 2010). In the last two decades, a lot of research has been carried out on these deposits and their related alteration zones (among others: Simmons et al., 2015; Abedini, 2017; Abedini et al., 2020). However, geochemical characteristics of hydrothermal alterations, especially argillic alteration,

* Corresponding author e-mail: abedini2020@yahoo.com

have not been much studied. In the northeast of the Kharvana city of the AHAVB, the emplacement of Oligocene intrusive rocks into Cretaceous volcanic rocks causes the generation and development of large-scale hydrothermal alterations (Jamali et al., 2010). The main hydrothermal alteration is the argillic alteration zone. The main goals of this study are to provide comprehensive information on factors controlling the mobility and concentration of REE and Eu and Ce anomalies during the development of the argillic alteration zone in the northeast of the Kharvana.

2. Geological Setting of the Study Area

According to the geological zones of Iran of Nabavi (1976), the study area is within the Alborz–Azarbaidjan structural zone (Figure 1). The oldest rock units are Cretaceous in age, from the oldest to the youngest, including andesite, limestone, and crystalline tuff interlayered with thin-bedded limestone. The Cenozoic lithological sequence includes Paleocence marl, shale, and limestone, Oligocene diorite, gabbro diorite, tonalite, granodiorite, and quartz diorite (Figure 2). Quaternary alluvial sediments are the youngest rock units in the Kharvana area.

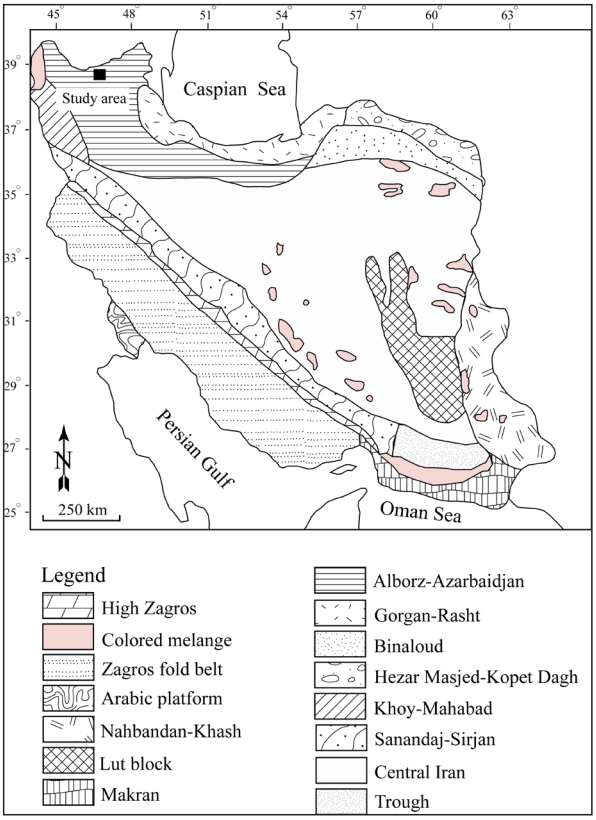

Figure 1. Zonal subdivisions of Iran (Nabavi, 1976); inset shows the location of the Kharvana area within the Alborz–Azerbaijan zone.

The emplacement of Oligocene tonalite, granodiorite, and quartz diorite plutons into Cretaceous andesitic rocks is associated with the development of large-scale argillic alteration zone (Jamali et al., 2010) (Figure 3a, b). Moreover, Cu–Fe skarn deposits are interpreted to have formed in the contact of the aforementioned intrusive suites and Cretaceous carbonate rocks. Coarse crystals of garnet, along with magnetite and chalcopyrite are observed in hand specimens of skarn samples.

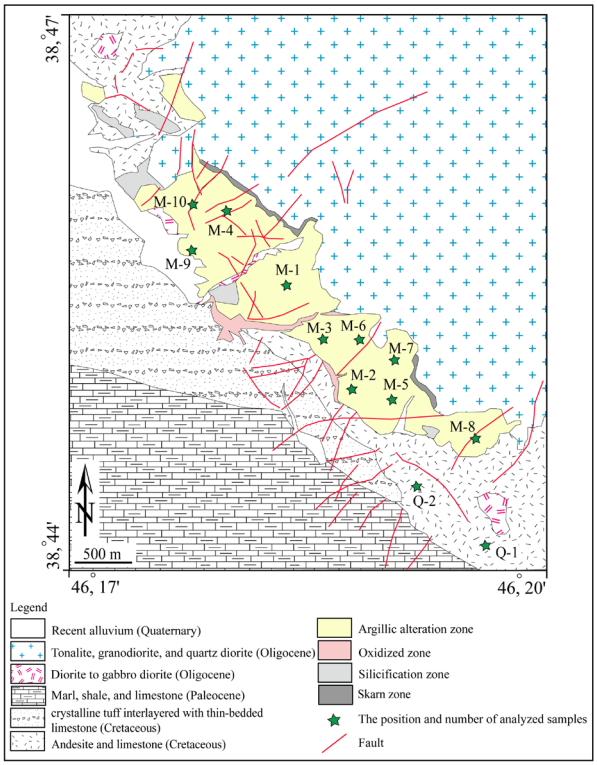

Figure 2. Simplified geological map showing lithological units and the distribution of argillic alteration zone for the northeast of the Kharvana area.

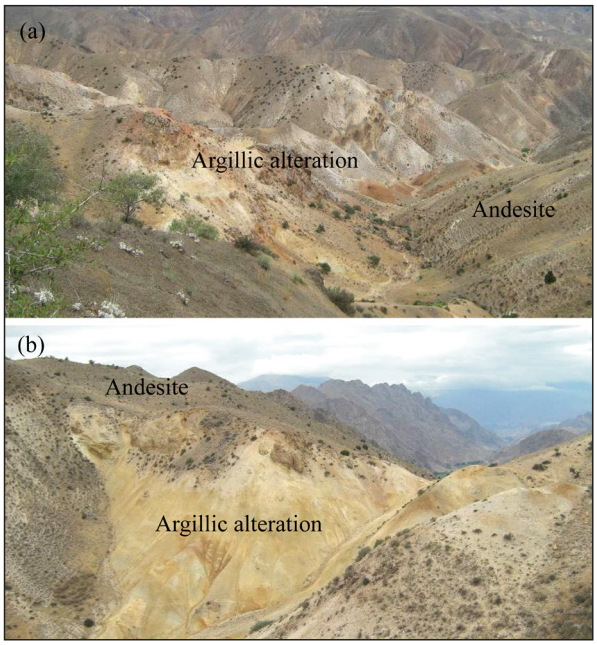

Figure 3. (a, b) The development of argillic alteration zone related to the andesitic rocks in the northeast of the Kharvana area (looking to the south).

Field surveys show that siliceous masses are developed on the argillic alteration zone. The occurrence of faults in the place where siliceous masses outcropped is indicative of Si leaching from the argillic alteration zone by hydrothermal fluids. Fe-bearing minerals, such as hematite, limonite, and jarosite, are also observed in the argillic alteration zone. The existence of chalcopyrite, pyrite, malachite, azurite, gypsum, anhydrite, and barite mineralizations as veins, veinlets, and breccia is other obvious geological characteristics of the argillic alteration zone in the northeast of the Kharvana area.

3. Sampling and Analytical Method

In this study, 12 representative samples were collected from different rock units. Microscopic studies of andesitic rocks were studied using an Olympus BX60F5 optical microscope at the Department of Geology of Urmia University, Iran. Mineralogical compositions of 10 argillic samples were obtained at the Geological Survey of Iran, Tehran by X-ray diffraction (XRD) with a Siemens D5000 X-ray diffractometer with the following operating conditions: Cu-Kα radiation at an accelerating voltage of 40 kV and a beam current of 40 mA, scanning speed of 2° per minute, and scan range of 2°–70°. Whole-rock geochemical analysis of all 12 samples (10 samples from the argillic alteration zone and 2 samples from the least-altered andesitic rocks) was carried out at the Activation Laboratories Ltd. (ALS Chemex, Vancouver, Canada). Major oxides and trace elements were analyzed by Inductively Coupled Plasma-Atomic Emission Spectrometry (ICP–AES) and Inductively Coupled Plasma-Mass Spectrometry (ICP–MS) respectively. The loss-on-ignition (LOI) was obtained by weight difference after ignition at 950 °C in a muffle furnace for 90 minutes. Results of geochemical analysis and LOI contents of samples from the argillic alteration zone and the least-altered volcanic rocks of the northeast of the Kharvana area are given in Table 1.

Table 1. Chemical analysis of major oxides and REE from the argillic alteration and the least-altered andesitic samples of the northeast of the Kharvana area, northwestern Iran.

		Andesite		Argillic alteration zone									
	DL	Q-1	Q-2	M-1	M-2	M-3	M-4	M-5	M-6	M-7	M-8	M-9	M-10
SiO_2 (wt%)	0.01	54.65	57.38	60.45	54.25	60.35	63.81	58.78	60.85	57.58	57.09	57.77	65.42
Al_2O_3	0.01	15.82	16.32	16.59	17.03	16.85	16.54	16.56	16.98	16.85	16.98	17.21	16.35
Fe_2O_3	0.04	8.51	7.06	5.06	8.85	6.21	4.02	6.88	3.35	8.84	7.26	7.09	3.16
MgO	0.01	6.58	4.65	0.22	0.51	0.45	0.19	0.54	0.61	0.56	0.61	0.61	0.74
CaO	0.01	7.91	7.55	0.12	0.15	0.13	0.11	0.12	0.16	0.12	0.13	0.14	0.08
Na_2O	0.01	3.55	3.69	0.24	0.29	0.26	0.22	0.23	0.32	0.23	0.27	0.29	0.16
K_2O	0.01	1.21	1.35	1.21	1.45	1.32	1.09	1.18	1.65	1.17	1.26	1.35	0.79
TiO_2	0.01	0.66	0.68	0.55	0.78	0.58	0.56	0.54	0.78	0.65	0.69	0.67	0.55
P_2O_5	0.01	0.28	0.29	0.06	0.23	0.19	0.14	0.18	0.18	0.19	0.16	0.12	0.09
MnO	0.01	0.07	0.09	0.23	0.11	0.12	0.07	0.16	0.17	0.08	0.08	0.07	0.03
LOI	–	0.75	0.91	15.2	16.3	13.3	13.1	14.7	14.9	13.7	15.3	14.6	12.6
Sum	–	99.99	99.97	99.93	99.95	99.76	99.85	99.87	99.95	99.97	99.83	99.92	99.97
La (ppm)	0.1	23.8	27.0	22.7	33.5	31.9	25.1	27.6	26.8	34.3	33.3	35.5	14.6
Ce	0.1	49.8	57.7	33.8	50.4	44.7	33.3	40.5	46.6	47.2	51.1	50.9	21.6
Pr	0.02	5.17	6.18	4.83	7.77	6.71	4.62	6.09	7.18	8.01	7.92	9.06	3.36
Nd	0.3	21.4	24.2	15.4	29.3	24.5	16.1	23.3	27.3	30.3	29.7	32.7	11.9
Sm	0.05	3.89	3.59	2.59	5.20	4.40	2.35	4.28	5.23	5.28	5.45	6.08	2.44
Eu	0.02	1.03	1.03	0.70	1.32	1.12	0.65	1.16	1.10	1.31	1.28	1.56	0.68
Gd	0.05	3.47	3.36	2.15	4.57	3.98	1.94	4.02	4.70	4.88	5.06	5.58	2.24
Tb	0.01	0.55	0.53	0.35	0.75	0.65	0.32	0.72	0.79	0.79	0.81	0.91	0.43
Dy	0.05	3.85	3.96	2.08	4.18	3.73	1.78	4.16	4.69	4.27	4.77	5.32	2.61
Ho	0.02	0.75	0.63	0.44	0.86	0.72	0.40	0.85	0.99	0.94	0.97	1.07	0.49
Er	0.03	1.94	2.15	1.36	2.50	2.27	1.24	2.51	2.97	2.67	2.70	2.90	1.63
Tm	0.1	0.32	0.29	0.22	0.39	0.35	0.22	0.39	0.47	0.41	0.44	0.46	0.29
Yb	0.05	1.87	1.95	1.51	2.49	2.30	1.45	2.57	3.18	2.64	2.87	2.86	1.81
Lu	0.01	0.33	0.29	0.25	0.41	0.39	0.24	0.43	0.50	0.42	0.45	0.46	0.29
ΣLREE (La–Eu) (ppm)	–	105.16	119.62	80.00	127.39	113.32	82.09	102.97	114.20	126.30	128.66	135.82	54.47
ΣHREE (Gd–Lu) (ppm)	–	13.08	13.16	8.36	16.13	14.38	7.59	15.63	18.28	17.02	18.07	19.57	9.79
ΣREE (La–Lu) (ppm)	–	118.24	132.78	88.36	143.51	127.70	89.68	118.60	132.48	143.32	146.73	155.39	64.26
Eu/Eu*	–	0.83	0.88	0.89	0.80	0.82	0.90	0.83	0.66	0.77	0.72	0.80	0.87
Ce/Ce*	–	0.98	0.99	0.71	0.69	0.67	0.66	0.69	0.75	0.63	0.70	0.63	0.68
$(La/Yb)_N$	–	8.62	9.34	10.16	9.10	9.37	11.70	7.25	5.70	8.77	7.83	8.40	5.43
$(\Sigma LREE/\Sigma HREE)_N$	–	3.53	3.99	4.20	3.46	3.46	4.74	2.89	2.74	3.26	3.12	3.04	2.44

Abbreviations: DL = detection limit, LOI = loss-on-ignition.
$Eu/Eu^* = Eu_N/(Sm_N \times Gd_N)^{1/2}$; $Ce/Ce^* = 2Ce_N/(La_N + Pr_N)$; $(La/Yb)_N = (La/Yb)_{samples}/(La/Yb)_{chondrite}$; $(\Sigma LREE/\Sigma HREE)_N = (\Sigma LREE/\Sigma HREE)_{samples}/(\Sigma LREE/\Sigma HREE)_{chondrite}$, where the subscript "N" refers to normalized values to chondrite (Taylor and McLennan, 1985).

Geochemical parameters, such as $(\Sigma LREE/\Sigma HREE)_N$ and $(La/Yb)_N$ ratios, are representative of the fractionation of REE during argillization of the andesitic rocks in the study area, where LREE and HREE are of La–Eu and Gd–Lu respectively. The Eu and Ce anomalies are calculated by the following equations of Taylor and McLennan (1985), where the subscript "N" indicates values normalized to chondrite.

$$Eu/Eu^* = Eu_N/(Sm_N \times Gd_N)^{1/2}$$

$$Ce/Ce^* = 2Ce_N/(La_N + Pr_N)$$

4. Results and Discussion

Microscopic observations show that the andesite rocks related to the argillic alteration zone have a porphyritic texture, in which phenocrysts are present in a fine-grained matrix. Plagioclase, pyroxene, and hornblende with up to 5 mm in the longest dimension are the most frequent phenocrysts of these rocks. Sometimes, these phenocrysts are altered into a series of clay minerals, chlorite, epidote, and sericite. Pyrite is the most important metal mineral present in these rocks. This mineral is observed as euhedral to subhedral crystals in the matrix.

According to PXRD analysis, quartz, kaolinite, and pyrophyllite are the main mineral assemblage of all the studied samples from the argillic alteration zone (Figure 4a, b). However, alunite, hematite, jarosite, goethite, muscovite–illite, rutile, pyrite, and chlorite are present at minor contents in the studied samples (Figure 4, b). The existence of pyrophyllite, alunite, jarosite, and rutile minerals shows that Cretaceous andesitic and andesitic–basaltic rocks have experienced an advanced argillic alteration, and the activity of sulfate ions in solutions responsible for alteration was high.

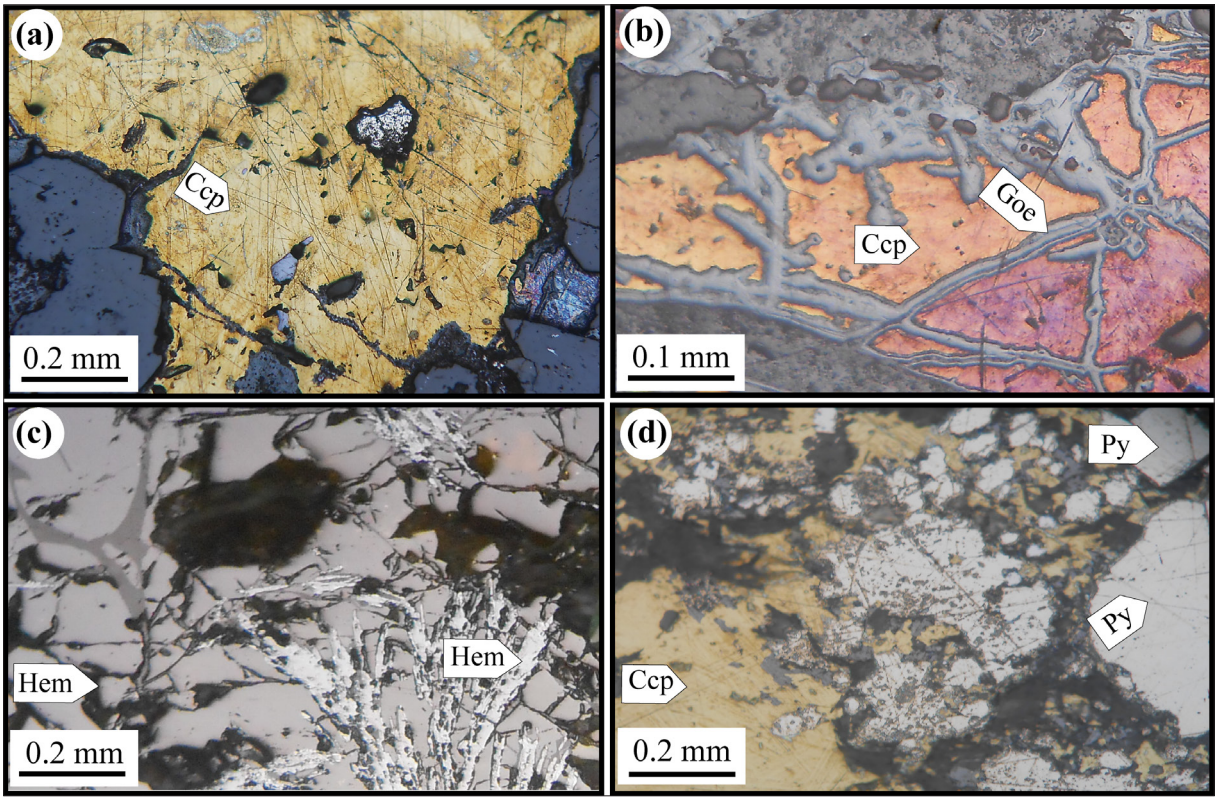

Figure 4. Photomicrographs of mineral phases in mineralized veins/veinlets from the Kharvana area. (a) Subhedral chalcopyrite crystal; (b) goethite in the rim of chalcopyrite; (c) elongated crystals of hematite; and (d) eudedral to subhedral pyrite. All photos are in reflected light. Abbreviations: Ccp = chalcopyrite; Goe= goethite, Hem = hematite, Py = pyrite.

Mineralogical studies show that the major minerals present in veins and veinlets of the argillic alteration zone are chalcopyrite, pyrite, malachite, azurite, and iron oxides and hydroxides, such as goethite, hematite, and limonite (Figure 5a–d). In microscopic sections, chalcopyrite shows no regular geometric shape (Figure 5a), but pyrite occurs as euhedral to subhedral crystals (Figure 5d) that are strongly tectonized. Hematite is observed as elongated crystals (Figure 5c). Sometimes, chalcopyrite is replaced by goethite during supergene processes (Figure 5b). Malachite and azurite accompanied with goethite are green and bluerespectively.

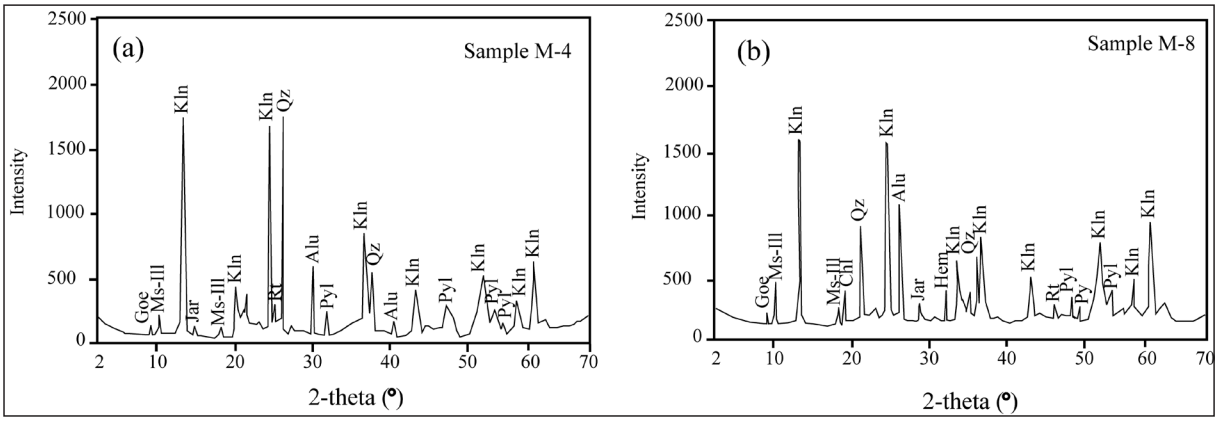

Figure 5. Powder-XRD patterns of the two-argillic samples from the Kharvana area. Abbreviations: Alu = alunite, Chl = chlorite, Goe = goethite, Hem = hematite, Jar = jarosite, Kln = kaolinite, Ms–Ill = muscovite–illite, Py = pyrite, Pyl = pyrophyllite, Qz = quartz, Rt = rutile.

So far, many methods have been presented for the calculation of mass changes of elements during alteration and/or weathering processes by different researchers. The most important methods are volume factor (Gresens, 1967), absolute weathering index (Nesbitt, 1979), isocon analysis (Grant, 1986), immobile elements (Brimhall and Dietrich, 1987; MacLean and Kranidiotis, 1987), percentage of changes in elemental ratios (Nesbitt, 1979; Nesbitt and Markovics, 1997), mobility index (Ng et al., 2001), chemical depletion fraction, and immobile plateau (Gong et al., 2011). In general, the calculation of mass change in these methods is similar to each other. However, the determination of immobile element(s) for the calculation of mass change is regarded as a key factor. Trace elements, such as Al (Duzgoren-Aydin et al., 2002) and Ti (Siahcheshm et al., 2014), are considered immobile elements during hydrothermal alteration processes. These trace elements have relatively high field strengths with restricted dissolution degrees in water (Little

and Aeolus, 2006). In this study, taking into account Al as a less-mobile element during the argillization of the andesitic rocks, the degree of mobility of REE was calculated by the following equation of Nesbitt (1979):

$$\text{Change} = [(X/Al)_{\text{argillic sample}}/(X/Al)_{\text{andesite}}] - 1 \times 100\%$$

where X is the concentration of the selected element.

Accordingly, negative and positive values indicate a loss and gain in the mass of REE during argillization of the andesite rocks respectively. The resultant results are given in Table 2 and shown in Figure 6. Among the lanthanides, only Ce shows a mass loss, and the rest of the lanthanides show both depletion and enrichment during the formation and evolution of the argillic alteration zone.

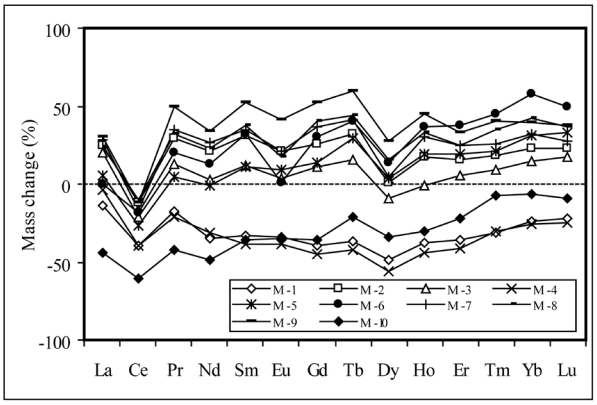

Figure 6. Mass changes of REE for the argillic alteration samples of the northeast of the Kharvana area.

Generally, low and high pH of the environment causes the leaching and precipitation of REE in alteration systems respectively (Patino et al., 2003). Based on mass changes of REE for the argillic alteration samples in Figure 6, except for Ce, which is depleted in all the samples, the behavior of lanthanides depends on the change of pH of solutions during argillization processes. Mass changes of REE show that REE in the argillic alteration samples developed near faults are leached, due to the low pH of alteration fluids. They are subsequently concentrated and enriched far away from faults, due to the decrease of temperature and high pH of alteration fluids.

Several minerals, such as kaolinite, Fe and Mn oxides and hydroxides, and secondary phosphates, are introduced as the main hosts of REE in alteration products (Höhn et al., 2014). Among the lanthanides, there are strong positive correlations among HREE (r = 0.94–0.99) compared to LREE (r = 0.63–0.99). The positive correlation between Al_2O_3 and REE (r = 0.93) (Figure 7a) probably represents the remarkable role of clays, especially kaolinite, in the distribution of REE. In addition, moderate positive correlations between REE and Fe_2O_3 (r = 0.73) (Figure 7b), TiO_2 (r = 0.69) (Figure 7c), and K_2O (r = 0.71) (Figure 7d) indicate that hematite and goethite, along with rutile, muscovite–illite, and jarosite possibly are other minerals controlling the distribution of lanthanides in the Kharvana alteration system. In the end, it can be concluded that factors, such as adsorption, scavenging, and isomorphic substitution, have important roles in the distribution and fractionation of REE in the Kharvana argillic alteration zone.

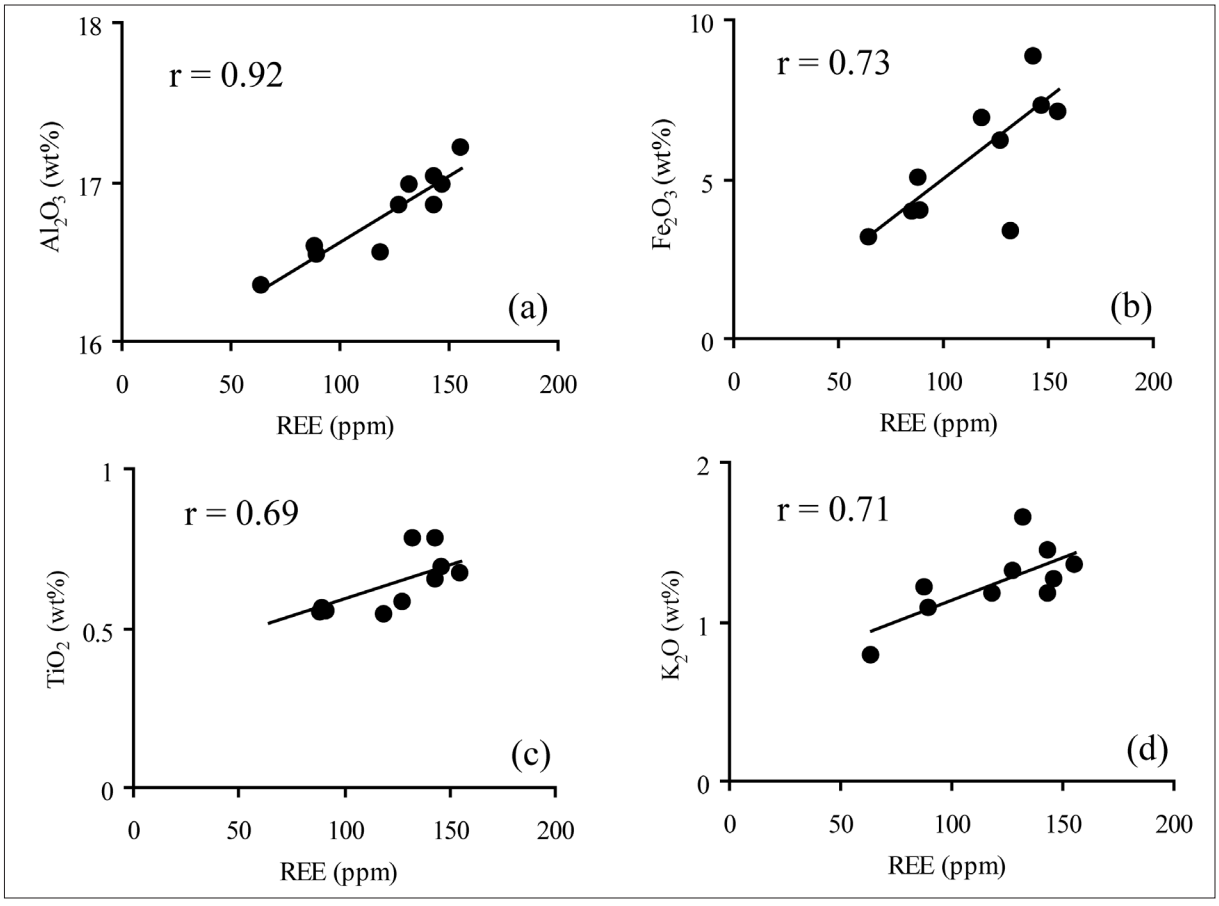

Figure 7. Bivariate diagrams of (a) Al2O3–REE, (b) Fe2O3–REE, (c) TiO2–REE, and (d) K2O–REE for the studied samples from the argillic alteration zone.

Chondrite-normalized REE spider diagrams in Figure 8 indicate fractionation and weak enrichment of LREE relative to HREE during the development of the argillic alteration zone. REE patterns for the andesitic rocks are almost similar to the argillic alteration samples, except for Ce anomaly that shows a significant negative anomaly in most of the argillic alteration samples. The ratios of $(\Sigma LREE/\Sigma HREE)_N$ and $(La/Yb)_N$ in the argillic alteration samples are within the range of 2.44–4.74 and 5.43–11.70 respectively. These ratios in the andesitic samples are from 3.53 to 3.99 for $(\Sigma LREE/\Sigma HREE)_N$ and 8.62 to 9.34 for $(La/Yb)_N$. These ratios show both an increase and decrease in content for the argillic alteration samples compared to the andesitic rocks, representing fractionation of LREE from HREE during the development of the argillic alteration zone in the study area. It is thought that fractionation of LREE from HREE during alteration processes depends on environmental pH. As a whole, LREE and HREE tend to be mobilized during acidic and alkalic pH respectively (Patino et al., 2003). The $(\Sigma LREE/\Sigma HREE)_N$ and $(La/Yb)_N$ decreasing trend in the argillic alteration samples at the contact of faults can be attributed to the low pH of hydrothermal fluids, as stated previously by Patino et al. (2003). The $(\Sigma LREE/\Sigma HREE)_N$ and $(La/Yb)_N$ increasing trend in the argillic alteration samples occurs far away from faults, due to the high pH of hydrothermal fluids. As a result, it seems that decreasing temperature and increasing pH of hydrothermal fluids, along with the destabilization of lanthanide complexes played important roles in an increase of $(\Sigma LREE/\Sigma HREE)_N$ and $(La/Yb)_N$ ratios in the Kharvana argillic alteration zone. In the end, it can be deduced that changes in the chemistry of solutions responsible for the alteration, such as a change in Eh and pH, and the difference in the degree of destabilization of lanthanide complexes are efficient parameters in REE distribution patterns during the development of the Kharvana argillic system.

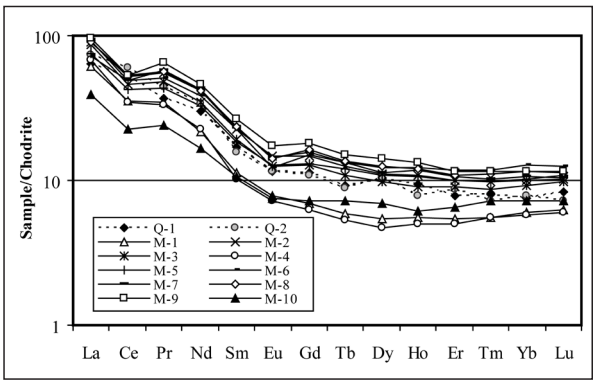

Figure 8. Chondrite-normalized REE spider patterns for the least-altered andesitic and argillic alteration samples.

The Eu and Ce anomalies in the argillic alteration samples are within the range of 0.59–0.86 and 0.63–0.78 respectively. These ratios in the andesitic samples are from 0.83 to 0.88 for Eu/Eu* and 1.02 to 1.03 for Ce/Ce*. The comparison of Eu and Ce anomalies between the argillic alteration samples and the least-altered andesitic samples from the northeast of the Kharvana area reveals that the argillization process of the andesites is accompanied by Eu and Ce negative anomalies. Negative Eu anomaly is attributed to the decomposition of plagioclase and hornblende of the andesitic rock at relatively high temperatures (e.g. Erkoyun and Kadir, 2011; Kadir et al., 2014), and negative Ce anomaly is indicative of a decrease in oxygen fugacity during the generation of argillic alteration zone in the Kharvana area (Burnham and Berry, 2014; Mondillo et al., 2016).

5. Conclusions

The most important conclusions of this study are as follows:

1- The presence of pyrophyllite, alunite, jarosite, and rutile minerals shows that the Cretaceous volcanic rocks have undergone advanced argillic alteration, and the activity of sulfate ion in solutions responsible for alteration was high.

2- Changes in pH and Eh of solutions responsible for alteration, along with the difference in the degree of destabilization of lanthanide complexes, adsorption, scavenging, and isomorphic substitution are the main factors controlling the distribution of REE in the argillic alteration system.

3- Accessory mineral phases, such as muscovite–illite, jarosite, hematite, goethite, and rutile, along with kaolinite played an important role in the distribution of lanthanides.

4- Negative Eu anomalies in the argillic samples are attributed to the decomposition of plagioclase and hornblende of the andesitic rocks by hydrothermal fluids.

5- Negative Ce anomalies in the argillic samples are indicative of a decrease in oxygen fugacity during alteration of the andesites.

Acknowledgments

The project was supported by the Bureau of Research Affairs of Urmia University, to which we are grateful. The authors acknowledge Prof. Eid Al-Tarazi, the Editor-in-Chief, and two anonymous reviewers for their insightful comments which helped to greatly improve the manuscript.

References

Abd El-Moghny, M. W., Abdel Hafez, N. A., Abuelleban, S. A. (2022). Geological, mineralogical and physical properties of Aswan kaolinitic clays, Egypt: Implications for industrial applications. Jordan Journal of Earth and Environmental Sciences 13: 64–73.

Abedini, A. (2017). Mineralogy and geochemistry of the Hizeh-Jan kaolin deposit, northwest of Varzaghan, East-Azarbaidjan Province, NW Iran. Iranian Journal of Crystallography and Mineralogy 24: 647–660.

Abedini, A., Calagari, A. A. (2012). The mineralogy and geochemistry of Permian lateritic ores in east of Shahindezh, West-Azarbaidjan province. Iranian Journal of Crystallography and Mineralogy 20: 59–72.

Abedini, A., Rezaei Azizi, M., Calagari, A. A. (2018). The lanthanide tetrad effect in argillic alteration: An example from the Jizvan district, northern Iran. Acta Geologica Sinica-English Edition 92: 1468–1485.

Abedini, A., Rezaei Azizi, M., Dill, H. G. (2020). The tetrad effect in REE distribution patterns: A quantitative approach to genetic issues of argillic and propylitic alteration zones of epithermal Cu–Pb–Fe deposits related to andesitic magmatism (Khan Kandi District, NW Iran). Journal of Geochemical Exploration 212: 106506.

Al Smadi, A., Al-Malabeh, A., Odat, S. (2018). Characterization and origin of selected basaltic outcrops in Harrat Irbid (HI), Northern Jordan. Jordan Journal of Earth and Environmental Sciences 9: 185–196.

Apollaro, C., Fuoco, I., Gennari, E., Giuliani, L., Iezzi, G., Marini, L., Radica, F., Di Luccio, F., Ventura, G., Vespasiano, G. (2023). Advanced argillic alteration at Cave di Caolino, Lipari, Aeolian Islands (Italy): Implications for the mitigation of volcanic risks and the exploitation of geothermal resources. Science of the Total Environment 889: 164333.

Brimhall, G. H., Dietrich, W. F. (1987). Constitutive mass balance relations between chemical composition, volume, density, porosity and strain in metasomatic hydrothermal systems: results on weathering pedogenesis. Geochimica et Cosmochimica Acta 51: 567–587.

Burnham, A. D., Berry, A. J. (2014). The effect of oxygen fugacity, melt composition, temperature and pressure on the oxidation state of cerium in silicate melts. Chemical Geology 366: 52–60.

Cravero, F., Marfil, S. A., Maiza, P. J. (2010). Statistical analysis of geochemical data: A tool for discriminating between kaolin deposits of hypogene and supergene origin, Patagonia, Argentina. Clay Minerals 45: 183–196.

Dill, G. D., Dohrmann, R., Kaufhold, S., Cicek, G. (2015). Mineralogical, chemical and micromorphological studies of the argillic alteration zone of the epithermal gold deposit Ovacik, Western Turkey: Tools for applied and genetic economic geology. Journal of Geochemical Exploration 148: 105–127.

Dill, H., Bosse, R., Henning, H., Fricke, A. (1997). Mineralogical and chemical variations in hypogene and supergene kaolin deposits in a mobile fold belt the Central Andes of northwestern Peru. Mineralium Deposita 32, 149–163.

Duzgoren-Aydin, N. S., Aydin, A., Malpas, J. (2002). Re-assessment of chemical weathering indices: Case study on pyroclastic rocks of Hong Kong. Engineering Geology 63: 99–119.

El-Hasan, T., Abdel-Haleem Al-Malabeh, A., Komuro, K. (2008). Rare earth elements geochemistry of the Cambrian shallow marine manganese deposit at Wadi Dana, South Jordan. Jordan Journal of Earth and Environmental Sciences 1: 45–52.

El-Hasan, T., Al-Malabeh, A. (2008). Geochemistry, mineralogy and petrogenesis of El-Lajjoun Pleistocene alkali basalt of Central Jordan. Jordan Journal of Earth and Environmental Sciences 1: 53–62.

Ercan, H. U., Ece, U. I., Schroeder, P. A., Karacik, Z. (2016). Differentiating styles of alteration within kaolin-alunite hydrothermal deposits of Çanakkale, NW Turkey. Clays and Clay Minerals 64: 245–274.

Erkoyun, H., Kadir, S. (2011). Mineralogy, micromorphology, geochemistry and genesis of a hydrothermal kaolinite deposit and altered Miocene host volcanites in the Hallaclar area, Uşak, western Turkey. Clay Minerals 46: 421–448.

Fulignati, P., Gioncada, A., Sbrana, A. (1999). Rare earth element (REE) behaviour in alteration facies of the active magmatic–hydrothermal system of Volcano (Aeolin Island, Italy). Journal of Volcanology and Geothermal Research 88: 325–342.

Galan, E., Aparicio, P., Gonzalez, I., Miras, A. (1998). Contribution of multivariate analysis to the correlation of some properties of kaolin with its mineralogical and chemical composition. Clay Minerals 33: 66–75.

Garofalo, P. S., Maffei, J., Paperschi, S., Dellistanti, F., Neff, C., Schwarz, G., Schmidt, P. K., Gunther, D. (2023). Fluid-rock interaction, skarn genesis, and hydrothermal alteration within an upper crustal fault zone (Island of Elba, Italy). Ore Geology Reviews 154: 105348.

Ghasemi Siani, M., Lentz, D. R. (2022). Lithogeochemistry of various hydrothermal alteration types associated with precious and base metal epithermal deposits in the Tarom-Hashtjin metallogenic province, NW Iran: Implications for regional exploration. Journal of Geochemical Exploration 232: 106903.

Gong, Q., Deng, J., Yang, L., Zhang, J., Wang, Q., Zhang, G. (2011). Behavior of major and trace elements during weathering of sericite-quartz schist. Journal of Asian Earth Sciences 42: 1–13.

Grant, J. A. (1986). The isocon diagram – A simple solution to Gresens' equation for metasomatic alteration. Economic Geology81: 1976–1982.

Grecco, L., Marfill, S., Maiza, P. J. (2012). Mineralogy and geochemistry of hydrothermal kaolins from the Adelita mine, Patagonia (Argentina); relation to other mineralization in the area. Clay Minerals 47: 131–146.

Gresens, R .L. (1967). Composition–volume relationships of metasomatism. Chemical Geology 2: 47–55.

Haas, J. R., Shock, E. L., Sassani, D. C. (1995). Rare earth elements in hydrothermal systems: estimates of standard partial modal thermodynamic properties of aqueous complexes of the rare earth elements at high pressures and temperatures. Geochimica et Cosmochimica Acta 59: 4329–4350.

Höhn, S., Frimmel H. E., Pašava, J. (2014). The rare earth element potential of kaolin deposits in the Bohemian Massif (Czech Republic, Austria). Mineralium Deposita 49: 967–986.

Jamali, H., Mehrabi, B. (2015). Relationships between arc maturity and Cu–Mo–Au porphyry and related epithermal mineralization at the Cenozoic Arasbaran magmatic belt. Ore Geology Reviews 65: 487–501.

Jamali, H., Dilek, Y., Daliran, F., Yaghubpur, A., Mehrabi, B. (2010). Metallogeny and tectonic evolution of the Cenozoic Ahar–Arasbaran volcanic belt, northern Iran. International Geology Review 52: 608–630.

Kadir, S., Ateş, H., Erkoyun, H., Külah, T., Esenli, F. (2022). Genesis of alunite-bearing kaolin deposit in Mudamköy member of the Miocene Göbel Formation, Mustafakemalpaşa (Bursa), Turkey. Applied Caly Science 221: 106407.

Kadir, S., Kulah, T., Eran, M., Önagil, N., Gurel, A. (2014). Minerlogical and geochemical characteristics and genesis of the Gözelyurt alunite-bearing kaolinite deposit within the late Miocene Gördeles ignimbrite, central Anatolia, Turkey. Clays and Clay Minerals 62: 477–499.

Karakaya, M. C., Karakaya, N., Kupeli, S., Yavuz, F. (2012). Mineralogy and geochemical behavior of trace elements of hydrothermal alteration types in the volcanogenic massive sulfide deposits, NE Turkey. Ore Geology Reviews 48: 197–224.

Karakaya, N. (2009). REE and HFS element behaviour in the alteration facies of the Erenler Dağı Volcanics (Konya, Turkey) and kaolinite occurrence. Journal of Geochemical Exploration 101: 185–208.

Little, M. G., Aeolus Lee, C. T. (2006). On the formation of an inverted weathering profile on Mount Kilimanjaro, Tanzania: Buried paleosol or groundwater weathering? Chemical Geology 235: 205–221.

MacLean, W. H., Kranidiotis, P. (1987). Immobile elements as monitors of mass transfer in hydrothermal alteration: Phelps Dodge massive sulfide deposit, Matagami, Quebec. Economic Geology 82: 951–962.

Mollai, H., Pe-Piper, G., and Dabiri, R. (2014). Genetic relationships between skarn ore deposits and magmatic activity in the Ahar region, Western Alborz, NW Iran. Geologia Carpathica 65: 207–225.

Mondillo, N., Boni, M., Balassone, G., Spoleto, S., Stellato, F.,

Marino, A., Santoro L., Spratt, J. (2016). Rare earth elements (REE)-minerals in the Silius fluorite vein system (Sardinia, Italy). Ore Geology Reviews 74: 211–224.

Nabavi, M. (1976). An Introduction to the Geology of Iran. Tehran, Iran. Geological Survey of Iran Publication (in Persian).

Nesbitt, H. W., Markovics, G. (1997). Weathering of granodioritic crust, long-term storage of elements in weathering profiles, and petrogenesis of siliciclastic sediments. Geochimica et Cosmochimica Acta 61: 1653–1670.

Nesbitt, H. W. (1979). Mobility and fractionation of rare earth elements during weathering of a granodiorite. Nature 279: 206–210.

Ng, C. W. W., Guan, P., Shang, Y. J. (2001). Weathering mechanisms and indices of the igneous rocks of Hong Kong. Quarterly Journal of Engineering Geology and Hydrogeology 34: 133–151.

Parsapoor, A., Khalili, M., Mackizadeh, M. A. (2009). The behaviour of trace and rare earth elements (REE) during hydrothermal alteration in the Rangan area (Central Iran). Journal of Asian Earth Sciences 34: 123–134.

Patino, L. C., Velbel, M. A., Price, J. R., Wade, J. A. (2003). Trace element mobility during spheroidal weathering of basalts and andesites in Hawaii and Guatemala. Chemical Geology 202: 343–364.

Qi-Cong, L., Cong-Qiang, L. (2002). Behaviour of the REE and other trace elements during fluid-rock interaction related to ore-forming processes of the Yinshan transitional deposit in China. Geochemical Journal 36: 443–463.

Seewald, J. S., Reeves, E. P., Bach, W., Saccocia, P. J., Craddock, P. R., Walsh, E., Shanks, W. C., Sylva, S. P., Pichler, T., Rosner, M. (2019). Geochemistry of hot-springs at the SuSu Knolls hydrothermal field, Eastern Manus Basin: Advanced argillic alteration and vent fluid acidity. Geochimica et Cosmochimica Acta 15: 25–48.

Siahcheshm, K., Calagari, A. A., Abedini, A., Sindern, S. (2014). Elemental mobility and mass changes during alteration in the Maher-Abad porphyry Cu–Au deposit, SW Birjand, Eastern Iran. Periodico di Mineralogia 83: 55–76.

Simmonds, V., Calagari, A. A., Kyser, K. (2015). Fluid inclusion and stable isotope studies of the Kighal porphyry Cu–Mo prospect, East-Azarbaidjan, NW Iran. Arabian Journal of Geosciences 8: 473–453.

Rezaei Azizi, M., Abedini, A., Slipour, S., Bagheri, H. (2018a). The Laal-Kan fluorite deposit, Zanjan Province, NW Iran: Constraints on REE geochemistry and fluid inclusions. Arabian Journal of Geosciences 11: 719.

Rezaei Azizi, M., Slipour, S., Abedini, A., Bagheri, H. (2018b). REE geochemical characteristics and fluid inclusion studies of the Bagher-Abad fluorite deposit, Central Iran. Neues Jahrbuch für Mineralogie-Abhandlungen 195: 247–263.

Tassongwa, B., Eba, F., Njoya, D., Tchakounte, J. N., Jeudong, N., Nkoumbou, C., Njopwouo, D. (2017). Physico-chemistry and geochemistry of Balengou clay deposit (West Cameroon) with inference to an argillic hydrothermal alteration. Comptes Rendus Geoscience 349: 212–222.

Taylor, Y., McLennan, S. M. (1985). The continental crust: Its composition and evolution, 1st ed. Oxford, UK: Blackwell.

Weimin, F., Corriveau, L., LaFlèche, M., Blein, O. (2003). Birdwing-shaped REE profile and or isovalent Nb/Ta, Zr/Hf ratios in the Bondy gneiss complex, Grenville Province, Québec: Sensitive geochemical markers of a fossil hydrothermal system in mineral exploration. Mining Industry Conference and Exhibition, Montreal 2003.

Wood, S. A. (1990). The aqueous geochemistry of the rare earth elements and yttrium: theorical prediction in hydrothermal solutions to 350 ºC at saturation of water vapour pressure. Chemical Geology 88: 99–125.